A Model of the Turbulent Diffusion of Bubbles below the Sea Surface

S. A. THORPE

Institute of Oceanographic Sciences, Wormley, Godalming, Surrey, GU8 5UB, U.K.

(Manuscript received 17 October 1983, in final form 13 February 1984)

ABSTRACT

Bubbles produced by breaking wind waves are carried by turbulence below the sea surface. In an earlier model of the distribution of bubble sizes with depth it was necessary to neglect certain terms in order to formulate a differential equation which was solved numerically. A model is devised in which this procedure is avoided. Turbulence is represented by a random walk or Monte Carlo simulation, and each bubble introduced at the surface is followed and a tally kept on its changing radius. Bubbles are continually introduced until a steady state is reached, when the distributions, gas fluxes, and acoustic scattering cross-sections are calculated. The results are compared with camera observations reported by Johnson and Cooke. The major contribution to both gas flux and to the acoustic scattering cross-section per unit volume at sonar frequencies of 248 KHz (corresponding to that which we have used to observe bubbles) comes from bubbles which, at the surface, have radii between ~40 and 100 μm. The model successfully reproduces the variation of the total number of bubbles with depth, but fails to describe the observed shape of the size distribution. Factors contributing to this discrepancy are discussed. It is possible that bubble populations measured by floating cameras are biased because of the effects of Langmuir circulation both on the float and on the bubbles.

1. Introduction

Subsurface bubbles formed by breaking wind waves have been subject to investigation for some time, primarily because of their role in the formation of aerosols when the bubbles burst on returning to the surface (Blanchard and Woodcock, 1957; Mason, 1971), but also because of their effect on underwater sound propagation (Urick, 1975), their action in scavenging particles or of creating particle amalgams when they dissolve (Johnson and Cooke, 1980), their production of foam (their surface counterpart, Monahan and O'Muircheartaigh, 1980) and their presence in spilling breakers (Longuet-Higgins and Turner, 1974). Interest in the downward diffusion of bubbles by turbulence, and the physics of "bubble clouds," has recently been excited by the discovery that they can be detected by subsurface, upward-pointing, sonar (Aleksandrov and Vaindruk, 1974; Thorpe, 1982, hereafter referred to as I; Thorpe and Hall, 1983). There is a need to devise reliable models of the bubbles if the sonar measurements are to be used to infer characteristics of the turbulence (Thorpe, 1984a) or the gas flux carried into the water via the bubbles (Thorpe, 1984b).

The equations representing the dynamics of bubbles, formulated in terms of their mean size distribution per unit volume and unit radius $N(a, z)$, where a is the radius of a bubble at depth z, were described by Garrettson (1973). In I the equations, in particular the terms representing the flux of N in radius space, were simplified by making assumptions about the relative scales over which contributing terms were supposed to vary and by neglecting terms representing bubble accelerations. Although these assumptions appeared reasonable, some doubt remained about their validity. There was also difficulty in modeling bubbles composed of more than one gas. We have therefore devised a more direct means of modeling the bubbles, one in which each bubble is represented by a particle, the motion of which is described using a Monte Carlo simulation. This formulation has the advantage that fluxes can be better represented, bubble composition can vary, and mean flows can easily be included. One such type of flow is that due to Langmuir circulations (Leibovich, 1983) and this aspect of the model will be described elsewhere (Thorpe, 1984c). The present formulation has the disadvantage of being appropriate only when the diffusion coefficient is uniform in depth. The technique of simulating a turbulent flow by random motions and of following individual particles is not new, but it appears not to have been tried before in this context and, as we have mentioned, avoids difficulties inherent in other methods.

The results will be compared with the observations made by Johnson and Cooke (1979, hereafter JC) using a camera supported by a surface float. Bubble size distributions were reported at three depths 0.7, 1.8 and 4.0 m, in winds of 11–13 m s^{-1}. The distributions peaked at all depths at radii of about 50 μm, and the numbers decreased rapidly on either side of the peak and also rapidly with depth. The camera could not resolve bubbles smaller than 17 μm. Discrepancies between these observations and the predictions of the model are found which draw attention to the need for a better understanding of the physics of the near-surface ocean and for more comprehensive observations of bubble distributions themselves.

2. The model

Several processes contribute to the way a small bubble moves in turbulent flow. The bubble rises under the action of buoyancy forces but responds to the turbulent motions which tend to advect it. Provided the bubble is sufficiently small in comparison with the Kolmogorov scale, as will generally be the case except perhaps in the breaking waves where there are large bubbles and large dissipation so that the turbulent scale is small, we may suppose that its motion u is the sum of the local turbulent fluctuations v and the vertical speed with which the bubble would rise in a quiescent fluid, $-w_b\mathbf{z}$, where $\mathbf{z}$ is the unit downward vector;

$$u = v - w_b\mathbf{z}. \qquad (1)$$

There are then those processes which change the radius, a, of the bubble, and hence w_b. There is compression under the combined effects of hydrostatic pressure (p) and surface tension (γ) and the loss of gas by diffusion across the surface of the bubble. Following the discussion in I (Section 3.2) we may write

$$\frac{da}{dt} = \dot{a}_1 + \dot{a}_2, \qquad (2)$$

where $\dot{a}_1$ is the rate of change of radius due to gas flux,

$$\dot{a}_1 = \frac{-3RT}{(3pa + 4\gamma)}\left\{D_1\mathrm{K}_1N_1\left[x\left(p + \frac{2\gamma}{a}\right) - p_{10}\right] + D_2\mathrm{K}_2N_2\left[(1 - x)\left(p + \frac{2\gamma}{a}\right) - p_{20}\right]\right\}, \qquad (3)$$

and $\dot{a}_2$ is the rate of change of radius due to pressure variation

$$\dot{a}_2 = \frac{-a^2}{3pa + 4\gamma}\frac{dp}{dt}. \qquad (4)$$

Here we have assumed that the bubble is composed of two gases, (subscript $i = 1, 2$) with partial pressures p_{i0} in the water far from the bubble, diffusivities D_i, adsorption coefficients, K_i, and Nusselt numbers N_i and that one gas has mole fraction x in the bubble (the other gas has $1 - x$) where

$$\frac{dx}{dt} = \frac{3RT}{a(pa + 2\gamma)}\left\{D_2\mathrm{K}_2N_2x\left[(1 - x)\left(p + \frac{2\gamma}{a}\right) - p_{20}\right] - D_1\mathrm{K}_1N_1(1 - x)\left[x\left(p + \frac{2\gamma}{a}\right) - p_{10}\right]\right\}. \qquad (5)$$

In (5) R is the gas constant (8.31×10^{-3} m^3 kPa K^{-1}) and T is the temperature (283 K). The dimensional coefficients are chosen to represent oxygen ($i = 1$) and nitrogen ($i = 2$). The values used are $D_1 = D_2 = 2 \times 10^{-5}$ cm^2 s^{-1}, $\mathrm{K}_1 = 0.49$ g m^{-3} kPa^{-1}, $\mathrm{K}_2 = 0.21$ g m^{-3} kPa^{-1}, and we take ν (kinematic viscosity) = 1.0×10^{-2} cm^2 s^{-1}, $\gamma = 3.6 \times 10^{-2}$ N m^{-1} and $g = 981$ cm s^{-2}. The value $x = x_0 = 0.215$ represents an air mixture of the gases. The value of w_b and the N_i depend upon the nature of the bubble surface. Generally bubbles in the ocean will be covered by a surface active film which inhibits tangential motion and causes the bubbles to behave dynamically like solid spheres. In clouds of bubbles other effects may be important, particularly coalescence and the dynamical interaction of bubbles, but provided the number of bubbles per unit volume and their volume fraction are small these may be neglected. These and other assumptions inherent in the modeling are discussed in detail in I and by Thorpe (1984d).

Turbulence is simulated in the numerical scheme by displacements of the water surrounding a bubble through a distance L in a random direction θ in y, z space at each time step. From (1) the horizontal and vertical bubble displacements (Δy, Δz) are then

$$\left.\begin{aligned}\Delta y &= L\sin\theta \\ \Delta z &= L\cos\theta - w_b\Delta t\end{aligned}\right\}, \qquad (6)$$

where w_b is a function of bubble radius. Following I we took

$$w_b = \frac{2}{9}\left(\frac{a^2g}{\nu}\right)[(\mathcal{Y}^2 + 2\mathcal{Y})^{1/2} - \mathcal{Y}], \qquad (7)$$

where $\mathcal{Y} = 10.82\nu^2/ga^3$, which represents the vertical speed of bubbles to within 20% if $a < 400$ μm. The effective vertical turbulent diffusion coefficient is

$$K_v = \frac{L^2}{4\Delta t} \qquad (8)$$

(see Csanady, 1973). The bubble radius is changed at each time step Δt by the first-order finite difference representation of (2) with values of N_i fitted to theoretical estimates as described in I;

$$N_i = \begin{cases} 1, & \text{if } a < 4.5 \\ 1.292P_i^{1/9}, & \text{if } 4.5 < a < 28.1 \\ (2/\pi)P_i^{1/3}, & \text{if } 28.1 < a, \end{cases} \qquad (9)$$

where a is measured in μm and $P_i = aw_b/D_i$, ($i = 1$, 2), are the Péclet numbers. We introduce bubbles of sizes $10m$ μm, $1 < m < M$ (with M usually chosen as 20, so that the largest are of radius 200 μm) at the surface, $z = 0$, at each time, $n\Delta t$, and follow them until they pass back through $z = 0$ or their radius becomes less than 1 μm, when they are lost from the system, or until a time $T = N\Delta t$, when a steady state is reached. Bubbles of size less than 1 μm dissolve very rapidly and contribute negligibly to the gas flux or to the sound scattering, having a radius much less than the resonant radius of the sonar we used. The model was tested with values of Δt between 1 and 5 s. A value $T = 400$ s was sufficient for a steady state to be reached for K_v in the range $64 < K_v$ (cm^2 s^{-1}) < 320. This is consistent with the estimates of bubble lifetimes by Blanchard and Woodcock (1957), those in I, and direct observations of the duration of bubble clouds, typically 1 min, by Thorpe and Hall (1983). It was necessary to introduce a large number of bubbles since a high proportion was quickly lost by returning to the surface. In most of the simulations described below, 600 bubbles of each size were introduced at $z = 0$ at each time step. For $64 < K_v$ (cm^2 s^{-1}) < 256, more than 98% of the bubbles introduced at the surface with radii > 100 μm have returned to $z = 0$ by time T; between 2 and 10% of the bubbles introduced with radii between 20 and 60 μm remain in the water or have dissolved.

The numerical scheme was first tested by fixing $w_b = 0.54$ cm s^{-1}, selected since this is the rise speed of bubbles of radius 50 μm (i.e., corresponding to the peak in the size distributions reported by JC), and by allowing each bubble to decay at a rate σ. This was chosen as 0.018 s^{-1} which gives results consistent with more complex simulations (Thorpe, 1984a) and bubble lifetimes of about 1 min. Diffusion can then be described analytically by an equation for the bubble concentration C per unit volume,

$$-w_b \frac{dC}{dz} = K_v \frac{d^2C}{dz^2} - \sigma C, \tag{10}$$

where K_v is independent of z. Eq. (10) has the solution $\ln C \propto -\alpha z$ where $K_v = w_b \alpha^{-1} + \sigma \alpha^{-2}$. The simulation was run with a range of values of N and Δt, and good agreement was found both for the form of the $\ln C$ versus z distribution and for the values of K_v determined from its slope and (8), provided $L/\Delta t > w_b$, i.e., that the effective turbulent velocity exceeds the rise speed. If it does not, no bubbles are carried below the surface.

As formulated, the model assumes that the numbers of bubbles generated at the surface by breaking waves are uniformly distributed in radius. This is unlikely to be the case. Certainly there must be an upper limit to the size of bubbles produced by spilling waves or overturning breakers; the trapped air pockets are finite. The larger bubbles will rapidly return to the surface or become unstable and produce a spectrum of small bubbles by fragmentation. The mean size distribution very close to the surface is unfortunately unknown. We might however fit our results to the measurements of JC at 0.7 m in winds of 11–13 m s^{-1}, or adopt some imaginary distribution, and we shall describe the effects of this selection in section 3.2. Since the JC data provide a suitable reference we have chosen to focus our results on the value $K_v = 180$ cm^2 s^{-1} which other models (Thorpe, 1984a) suggest is an appropriate value for winds of about 12 m s^{-1}. We shall also present results predicting the bubble distributions at the three depths 0.7, 1.8, 4.0 m at which JC's measurements were made. In particular we assess the importance of each bubble size, $10m$ μm, introduced at the surface. We shall show how they determine the distribution of bubbles at depth and contribute to the gas flux and to the acoustic scattering cross-section per unit volume M_v. This is defined as a sum over the bubbles contained in a unit volume at time T of σ_1, the bubble scattering cross section, where

$$\sigma_1 = \frac{4\pi a^2}{(1 - \omega_0^2/\omega^2)^2 + \delta^2}. \tag{11}$$

Devin (1959) gives values of the damping coefficient δ; ω is the sonar frequency, 248 KHz, and ω_0 is the bubble resonant frequency

$$\omega_0 = \frac{1}{2\pi a}\left(\frac{3\gamma' p}{\rho}\right)^{1/2}, \tag{12}$$

where γ' is the ratio of specific heats, c_p/c_v, and ρ the density of water. In practice we estimate M_v by summing σ_1 over the bubbles within ± 10 cm of the depth level at which M_v is to be determined and by taking the appropriate average. The gas flux is similarly a sum at time T of the flux occurring from each bubble which then remains in $z > 0$.

3. Results

a. *Uniform input of bubbles*

Figure 1 shows the number of bubbles in each 10 μm size range within ± 10 cm of the three reference depths. In this case 1200 bubbles of each size were released at the surface at each time interval with $\Delta t = 5$ s. We took $K_v = 180$ cm^2 s^{-1} and both gases were 100% saturated in the water, so that $p_{10} = 0.215 p_0$ and $p_{20} = 0.785 p_0$, where p_0 is atmospheric pressure. The percentage super-saturation levels (s_i) are given by $s_1 = 100 p_{10}/x_0 p_0$, $s_2 = 100 p_{20}/[p_0(1 - x_0)]$, so that $s_1 = 3$ implies an oxygen saturation level in the water of 103%. Very small bubbles dissolve rapidly [$\dot{a}_1 \propto a^{-1}$ in (3) for small a] while large bubbles, having the largest w_b, return quickly to the surface and are lost. The distributions at each depth thus have a peak, and Fig. 1 shows that this tends to smaller radii as depth increases. The total number of bubbles decreases rapidly with depth, the effect being most notable for the larger bubbles which are absent at 4 m. The lines joining the crosses are labeled with values of m, and indicate the contribution to each 10 μm bubble size range from bubbles of size $10m$ μm introduced at the surface. At 0.7 m this contribution is primarily to a size range within 30 μm of the size of the bubble at the surface. At 1.8 m the major contribution at each size comes from bubbles which, at the surface, were at least 10 μm larger. The major contributions at 4.0 m are from

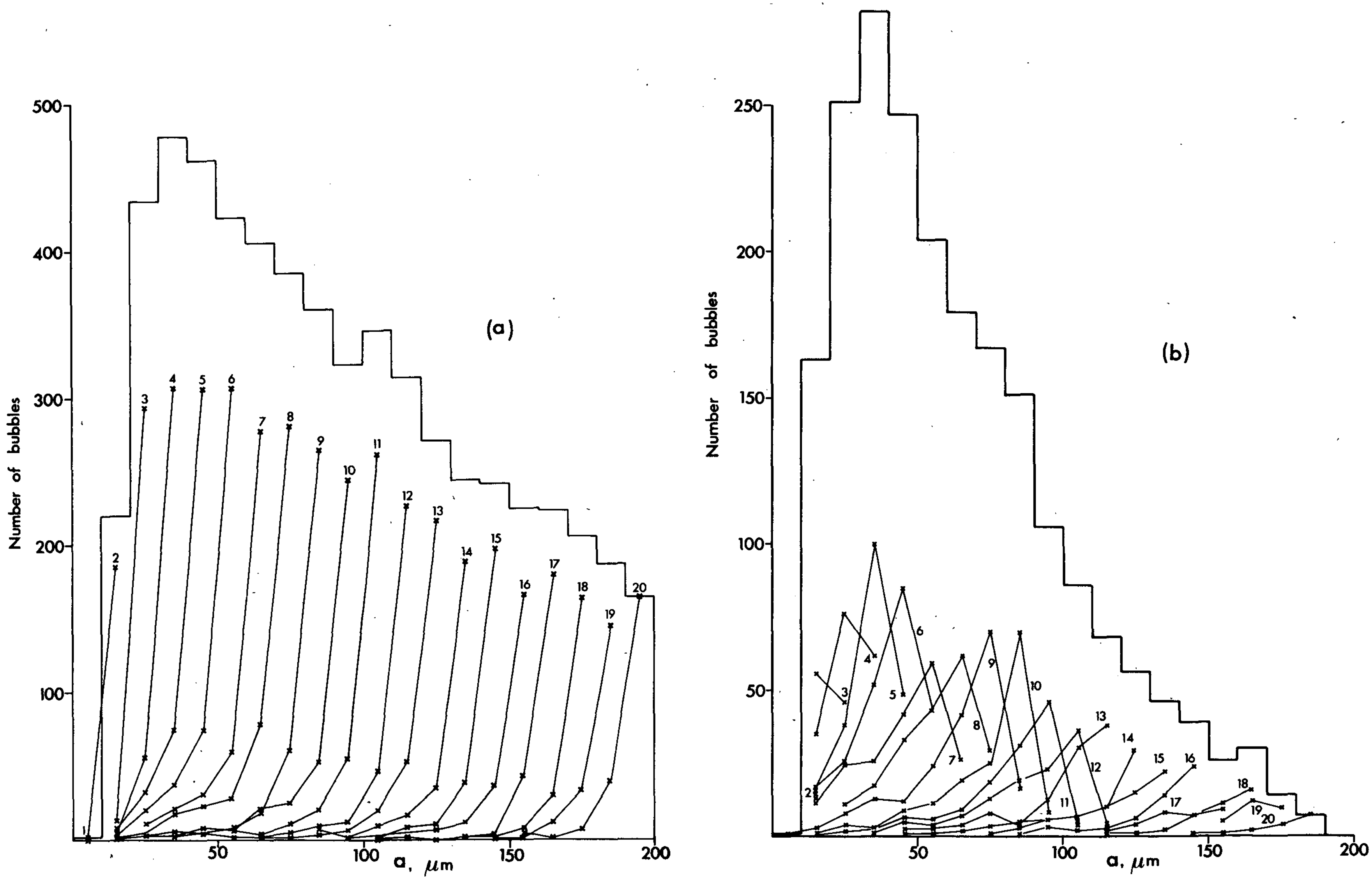

FIG. 1. Histograms of bubble numbers at (a) 0.7 m (b) 1.8 m and (c) 4.0 m in 10 μm size bands when 1200 bubbles of each size are introduced at each time step; $K_v = 180\ cm^2\ s^{-1}$, $s_1 = s_2 = 0$. The crosses represent the contributions from the bubbles of each radius size (10 × number shown, units μm) at the surface. In (c) contributions of less than 3 bubbles are not shown.

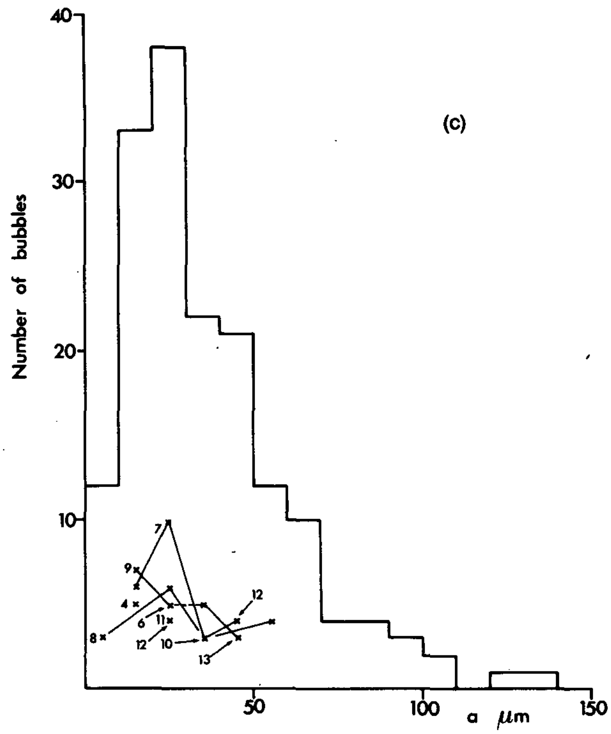

FIG. 1. (*Continued*)

bubbles which at the surface have radii between 60 and 100 μm.

The ordinate in Fig. 2 represents the contribution to the flux into the water of nitrogen F_N, from bubbles for each input size m when 600 bubbles of each size are introduced at each time step, $\Delta t = 5$ s. Again $K_v = 180$ cm^2 s^{-1}, but here various values of s $(=s_1 = s_2)$ are shown. As the saturation level increases the flux at all sizes decreases, eventually becoming negative for large bubbles which thus remove gas from the water (see Wyman *et al.*, 1952, and I for further discussion of this effect). In Fig. 3 we show the histogram of bubble numbers per 10 μm range at the three depths for values of $s = s_1 = s_2$ between −3 and +9. The distributions appear to be substantially independent of s, at least up to $s = +6$, approximately the same number of bubbles appearing in each radius bin with no systematic trends, in spite of the changes in net flux. There seem however to be rather fewer bubbles in the 20–100 μm band when $s = +9$.

Figure 4 shows the contributions to the scattering cross sections M_v at each depth from the bubble whose sizes, when introduced at the surface, were $10m$ μm; M_v increases with m at 0.7 m. At radii much greater than the resonant bubble radius,

$$a_r = \frac{1}{2\pi\omega}\left(\frac{3\gamma' p}{\rho}\right)^{1/2} \quad (13)$$

(about 14 μm at 1 m depth when $\omega = 248$ KHz), the scattering cross-section σ_1 (11) is approximately $4\pi a^2$, and so M_v is approximately equal to the area of the bubbles. The figure shows that at 0.7 m the area of bubbles increases with $m > 5$. At 1.8 m the area is almost independent of m. The scattering cross sections and the areas decrease rapidly with depth.

The figures show however that an input distribution of bubbles which is independent of size m provides far too many large bubbles in relation to those of radii near 50 μm. The ratio of the numbers of bubbles observed by JC at 0.7 m having radii between 42 and 60 μm to those between 196 and 212 μm was about 100:1. This ratio is only about 2.5:1 in Fig. 1a. We shall bias the input to reflect the observed trend. This is also necessary to remove the divergent trend of M_v with increasing m shown in Fig. 4 at 0.7 m.

b. *Input varying with bubble radius*

To find the appropriate bias to apply to the surface input of bubbles so that their summed contributions fit a particular distribution at depth (e.g., JC at 0.7 m), it is necessary to solve a set of simultaneous equations. If the distribution to be fitted is $P(n)$, $1 \leqslant n \leqslant n_{\max}$, where P is the number of bubbles per unit volume in the radius band $10(n-1) < a\,(\mu\mathrm{m}) < 10n$, and if from the given surface input there are $Q(m, n)$ bubbles found at the depth per unit volume per radius band $[10(n-1) < a\,(\mu\mathrm{m}) < 10n]$ from input at radius $10m$ μm, $m \leqslant 20$, then we need to find bias factors $r(m)$ such that

$$P(n) = \sum_m r(m)Q(m, n), \quad n = 1, 2, \ldots, n_{\max}. \quad (14)$$

Unless the bubbles introduced at the surface can grow, and this may occur under our assumptions only if s_1 or $s_2 > 0$, $n_{\max}$ must be $\leqslant 20$. Moreover the solutions must be such that $r(m) \geqslant 0$ for all m; we cannot introduce a negative number of bubbles. (We do not impose a control on the net flux of a particular size across the surface. There could be an efflux at a particular size which exceeded the production by breaking waves of bubbles at that size.)

We have used for $P(n)$ a smoothed version of JC's data at 0.7 m, interpolated to 10 μm wide radius bands and truncated at 200 μm, but conserving the total number of bubbles per unit volume, 4.8×10^5 bubbles m^{-3}. This is shown in Fig. 5b together with a linear distribution with the same total number of bubbles (marked by circles) and the distribution already shown in Fig. 1a resulting from a uniform surface input, but scaled to have the same total number of bubbles (marked by crosses). The value of K_v here is 180 cm^2 s^{-1} and $s_1 = s_2 = 0$. In this case it was possible to solve (14) for both the JC profile and the linear distribution and Fig. 5a shows the relative numbers of bubbles of each size n, proportional to the bias factors $r(m)$, needed to produce the distributions at 0.7 m. The crosses show

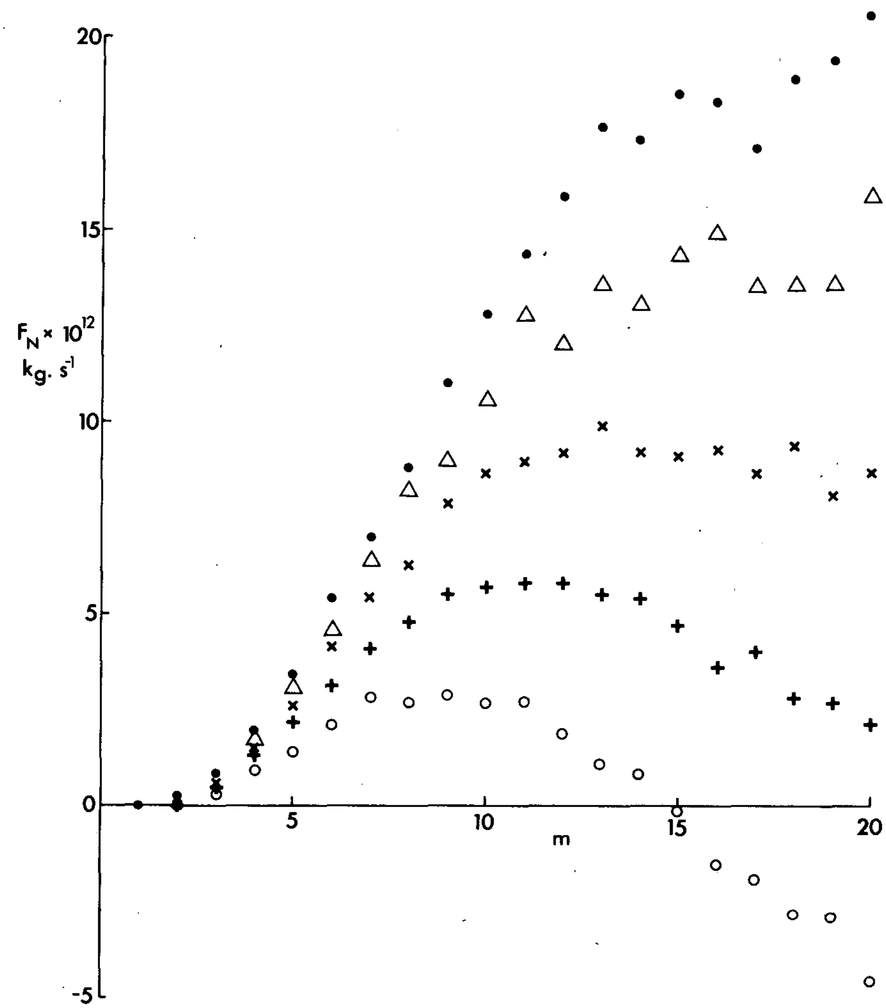

FIG. 2. The flux of nitrogen F_N from bubbles of each radius size m introduced at the surface, when 600 bubbles of each size are introduced at each time step $\Delta t = 5$ s, $K_v = 180$ cm^2 s^{-1}. The points represent different saturation levels $s = s_1 = s_2$: −3 (solid circles); 0 (open triangles); 3 (crosses); 6 (plus signs); 9 (open circles).

the uniform distribution. The numbers for the linear distribution (the circles in Fig. 5a) generally decrease as radius increases, but less rapidly than in Fig. 5b. This is because the numbers in the distribution in Fig. 1a, from which the bias factors at 0.7 m are deduced, itself decreases with $a > 30$ μm. In Fig. 5c the JC distribution has a peak just as it does at 0.7 m, but tends to become almost uniform for $15 < m < 20$.

We have used the calculated $r(m)$ to determine the corresponding distributions of bubbles at 1.8 and 4 m and have compared them with similarly smoothed versions of JC's data. The four distributions in Fig. 5(c and d) are the JC data, drawn as stepped histograms, and the three distributions resulting from uniform input (crosses), or fits to JC or the linear profile in (b). At 1.8 m (Fig. 5c) we see that the points fitted to JC at 0.7 m follow the data histogram for $a > 50$ μm fairly well, but have a peak at a lower radius where values exceed those observed. The other distributions have total numbers of bubbles which agree well with the observations. This is also the case at 4 m (Fig. 5d). Here however between 40 and 80 μm there are fewer bubbles in all simulations than JC observed and the simulations have similar distributions, all of which peak near 30 μm.

The differences between the simulated distributions and the observations are significant and we shall return to discuss this later. In Figs. 6 and 7 we examine the effect of varying D_i and K_v. The distributions are again first fitted to JC at 0.7 m and then corresponding distributions found at 1.8 and 4.0 m. Fig. 6 shows these when the values of the molecular diffusivity, D, taken to be the same for both gases, is halved or doubled. We have also shown the effect of making $D = 0$ for $a < 28.1$ μm to simulate bubbles which are so thickly covered by surface active contaminants that diffusion

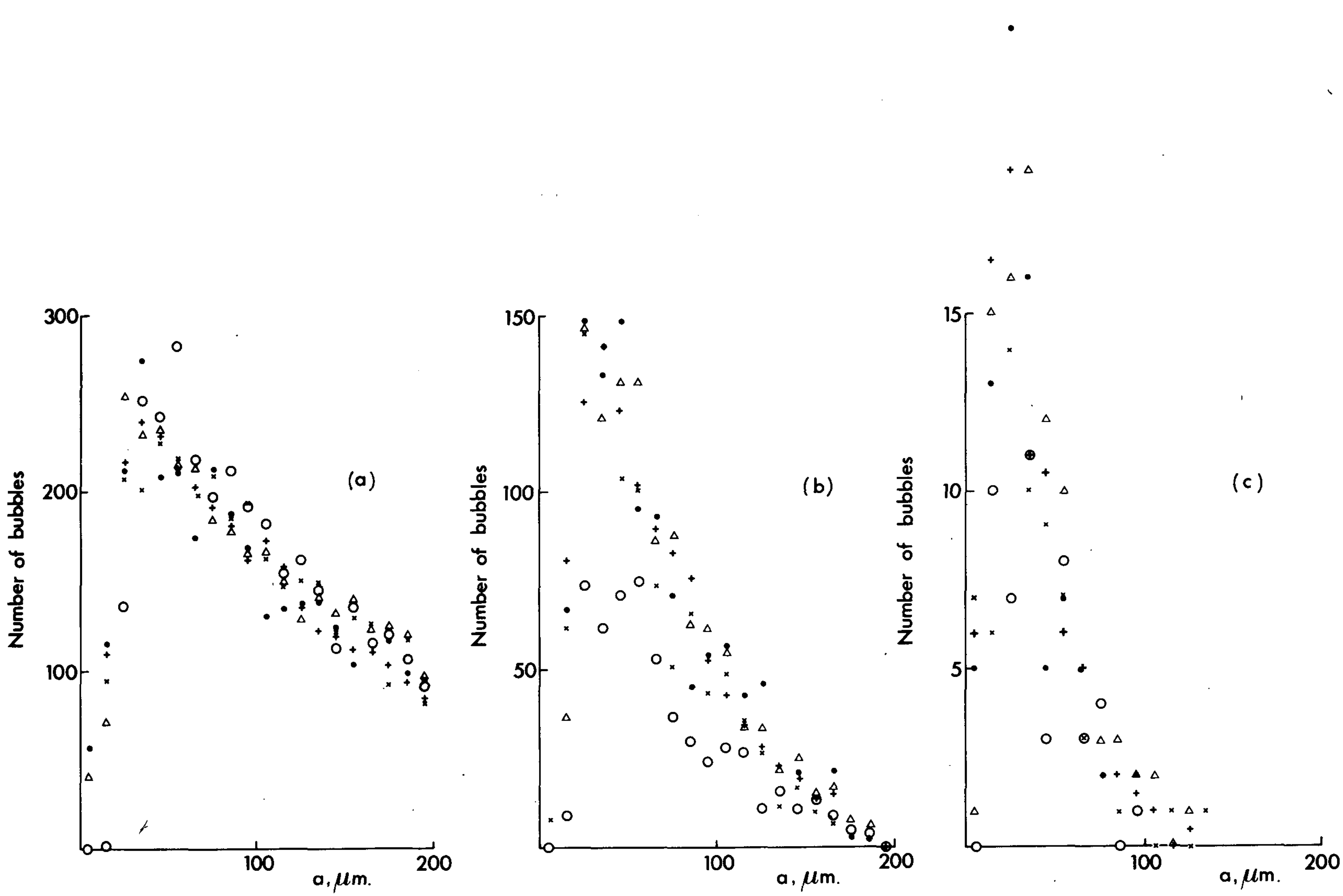

FIG. 3. Histograms of bubble numbers in 10 μm radius intervals (shown for clarity by points rather than by a stepped distribution) at (a) 0.7 m, (b) 1.8 m and (c) 4.0 m in 10 μm size bands when 600 bubbles of each size are introduced at each time step; K_v = 180 cm^2 s^{-1} and various values of $s = s_1 = s_2$ are shown: −3 (crosses); 0 (plus signs); +3 (closed circles); +6 (triangles); +9 (open circles).

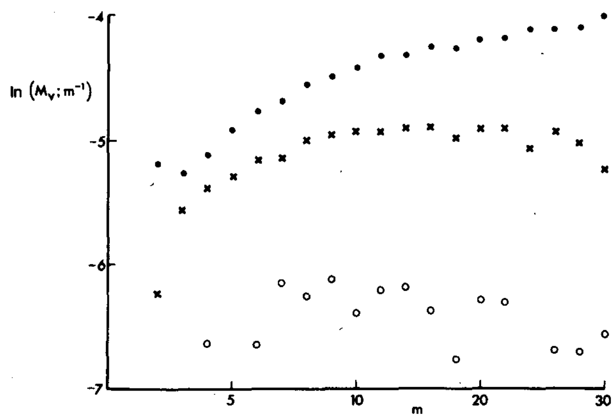

FIG. 4. The scattering cross-section per unit volume M_v from each radius size m introduced at the surface when 1200 bubbles of each size are introduced at each time step Δt = 5 s. K_v = 180 cm^2 s^{-1}, $s_1 = s_2 = 0$. The points are values at: 0.7 m (solid circles); 1.8 m (crosses); and 4 m (open circles) depth; lnM_v is plotted.

is totally inhibited. The principal effect of these changes is to raise or lower the distribution, and none are effective in increasing the radius at which the peak occurs. The total number of bubbles corresponds most closely to observations when D is about 2×10^{-5} cm^2 s^{-1}, the chosen value. The effect of variations in K_v on the bubble distribution is shown in Fig. 7. An increase in K_v produces an increase in the number of bubbles found at the lower reference depths. (The numbers introduced at the surface are not held constant. It is the distribution at 0.7 m which is fixed). The position of the peak is not however changed significantly.

The variation of gas flux with K_v, D ($=D_1 = D_2$) and s ($=s_1 = s_2$) is shown in Fig. 8. Fluxes for oxygen and nitrogen are shown separately, and two curves are shown for each. The full line represents a fit to the JC data at 0.7 m. The dashed lines are estimates calculated by using the bias factors determined from the JC data at 0.7 m with K_v = 180 cm^2 s^{-1}, $D = 2 \times 10^{-5}$ cm^2

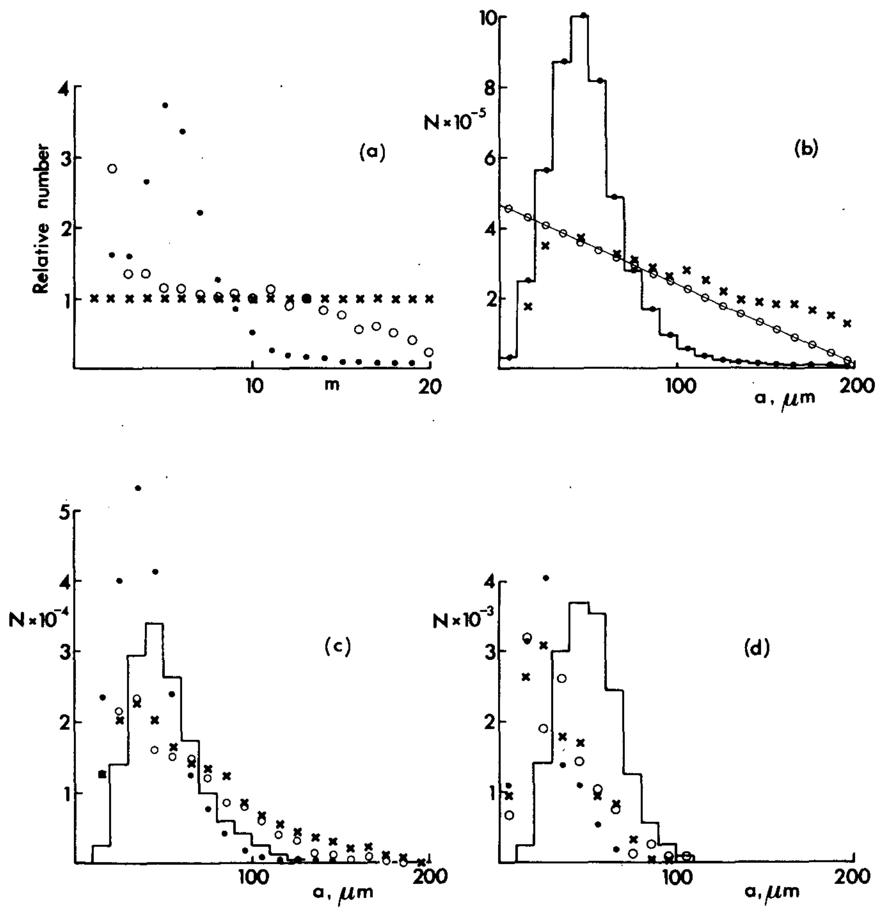

FIG. 5. (a) The relative numbers of bubbles introduced at the surface at each time step as a function of size m. The crosses show a uniform input. The open circles show the relative numbers needed to produce the linear trend in the histogram (b) at 0.7 m, while the dots are the relative numbers needed to produce the stepped histogram in (b), a smoothed version of Johnson and Cooke's data also shown at 1.8 m in (c) and 4.0 m in (d). The points in (c) and (d) represent the distributions corresponding to those shown in (b). N is the number of bubbles per cubic meter.

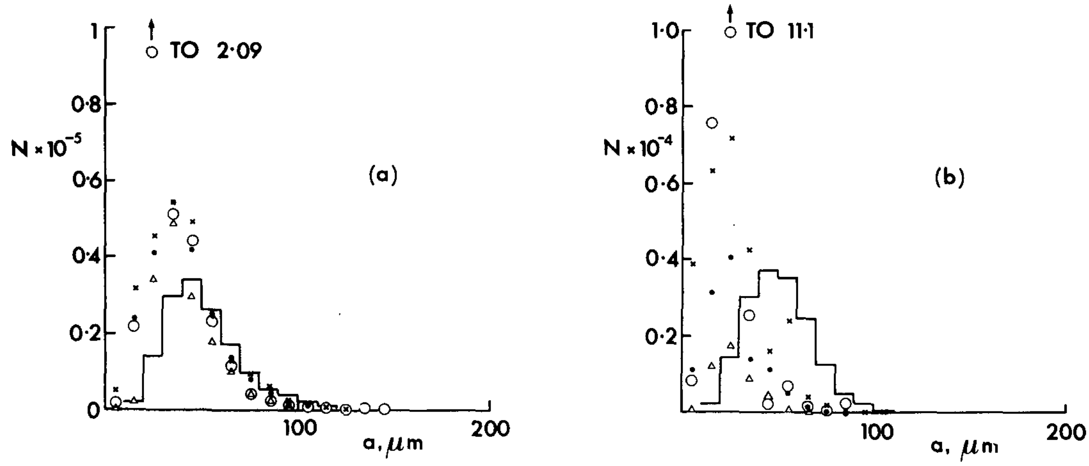

FIG. 6. Histograms of bubble numbers at (a) 1.8 m and (b) 4.0 m for K_v = 180 cm^2 s^{-1}, $s_1 = s_2 = 0$, when D (=D_1 = D_2) is varied. The stepped histograms represent Johnson and Cooke's data. The points are: (crosses) $D = 1 \times 10^{-5}$ cm^2 s^{-1}; (solid circles) $D = 2 \times 10^{-5}$ cm^2 s^{-1}; (triangles) $D = 4 \times 10^{-5}$ cm^2 s^{-1}; (open circles) $D = 0$ for $a < 28.1$ μm, $D = 2 \times 10^{-5}$ cm^2 s^{-1} for $a \geq 28.1$ μm. N is the number of bubbles per cubic meter.

s^{-1} and $s = 0$; this surface input, $S(m)$, is thus independent of K_v, D, or s. Changes in salinity may however have a profound effect on the bubble size distribution, and influence D and s. Far more small bubbles result from waves breaking in saline water than in fresh (see Scott, 1975) and, as shown in I, this has a significant effect on sound scattering. It seems likely that fewer bubbles result from breaking waves in fresh water because bubble coalescence is more frequent there (Lessard and Zieminski, 1971). Coalescence increases with rising temperature (Drogaris and Weiland, 1983) which will also affect D and s. Temperature variations affecting the stability of the atmospheric boundary layer may also result in changes in the frequency of breaking waves (Wu, 1979). It is not realistic to assume that the number of bubbles produced per unit area per unit time by breaking waves will generally be independent of K_v. Both increase with wind speed, and thus the individual estimates of fluxes in Fig. 8(a) must be scaled by some factor which also depends on wind in some

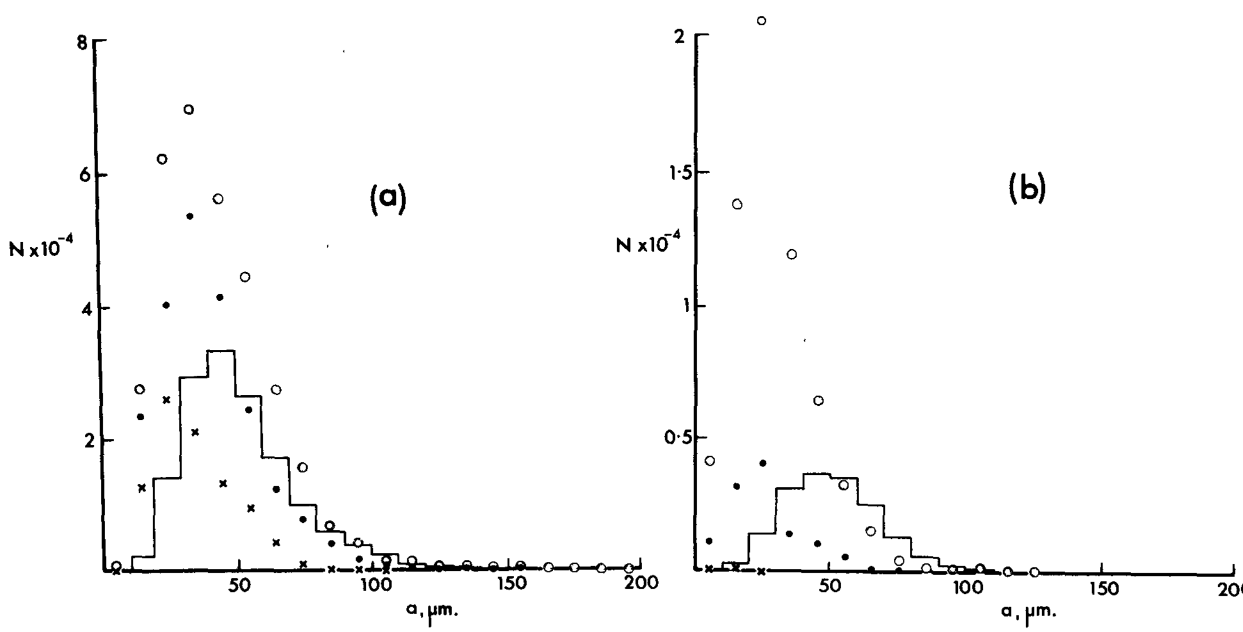

FIG. 7. Histograms of bubble numbers at (a) 1.8 m and (b) 4.0 m for $s_1 = s_2 = 0$ when K_v is varied. The stepped histograms represent Johnson and Cooke's data. The points are: (crosses) K_v = 80 cm^2 s^{-1}; (solid circles) K_v = 180 cm^2 s^{-1}; (open circles) K_v = 320 cm^2 s^{-1}. For K_v = 80 cm^2 s^{-1} very few bubbles reach 4 m depth. N is the number of bubbles per cubic meter.

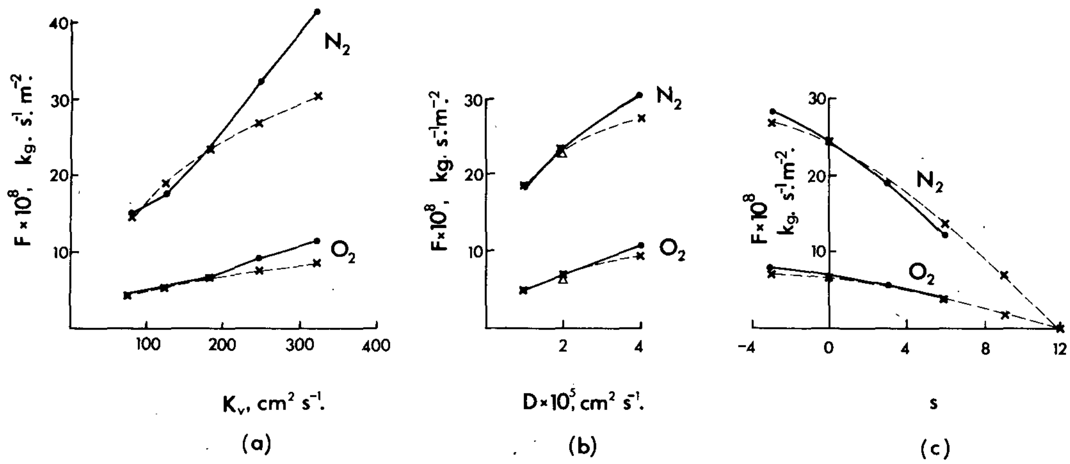

FIG. 8. The variation of gas flux (F) with (a) K_v (at $D = 2 \times 10^{-5}$ cm² s⁻¹, $s = 0$) (b) D (at $K_v = 180$ cm² s⁻¹, $s = 0$) and (c) s (at $K_v = 180$ cm² s⁻¹, $D = 2 \times 10^{-5}$ cm² s⁻¹) for oxygen and nitrogen. The full line joining the dots are from fits to Johnson and Cooke's distributions at 0.7 m. The dashed lines joining crosses are estimates based on the same input (S) of bubbles at the surface. The triangle in (b) marks the flux estimated when D is set to zero for <28.1 μm as in Fig. 6.

unknown way and which represents the increasing number of bubbles produced by breaking waves. There are two factors which may contribute. As wind increases, waves break more frequently (Thorpe and Humphries, 1980). Since the rms wave amplitude increases, it is probable that the breaking waves engulf a greater volume of air and become, on average, more efficient producers of bubbles. An indication of the net bubble production is provided by the observed increase in the area of floating foam with wind speed (Monahan and O'Muircheartaigh, 1980), although a definite relationship between foam and the subsurface bubble population has not been established.

Given however a constant bubble distribution at 0.7 m or a constant surface input S the curves of Fig. 8 show that the gas fluxes increase with D and K_v, and decrease with s. The solution of (14) at $s = 9$ produces negative bias factors when a fit is attempted to the JC data at 0.7 m. The dashed curves fitted to the points show that the fluxes become zero at about $s = 12$.

Figure 9 shows the contribution to the nitrogen flux from each surface bubble size, m, with variation in s (compare with Fig. 2). The gas flux is predominantly carried by bubbles which, at source, have radii between 40 and 100 μm. The slow convergence near $m = 20$ suggests that, due to truncation at 200 μm, the values in Fig. 8 may underestimate the flux by about 5×10^{-8} kg m⁻² s⁻¹ at $s = -3$.

The contribution to M_v at 1.8 m from bubbles of input size m is shown in Fig. 10 using again the surface input S for various K_v. The main contribution is from bubbles of sizes between 30 and 100 μm. Figs. 11a–c, shows the variation of $\ln M_v$ with depth for various values of K_v, D and s, again using S. The curves are all concave upwards and the slopes increase with K_v, D and s. If

$$d \equiv \left(-\frac{d}{dz}\ln M_v\right)^{-1} \tag{15}$$

is the inverse slope at 2 m we find, for variations ΔK_v, ΔD and Δs near $K_v = 180$ cm² s⁻¹, $D = 2 \times 10^{-5}$ cm² s⁻¹, and $s = 0$, that $\alpha = 0.81$ m and the variation Δd is approximately given by

$$\Delta d(m) = 0.023\Delta s + 0.26\frac{\Delta D}{D} + 0.74\frac{\Delta K_v}{K_v}. \tag{16}$$

Fig. 11d shows M_v as a function of depth but for a *uniform* input of bubbles at the surface (i.e. the crosses in Fig. 5a). Here M_v is normalized to unity at 1 m. The curves are more nearly linear than in (a) and at $K_v = 180$ cm² s⁻¹, d is now 0.79 m and $\Delta d(m) = 0.61\Delta K_v/K_v$.

4. Discussion

The gas flux and M_v are related. For $a > 28.1$ μm, $N_i \propto P_i^{1/3}$ (from 9) or, using (7), $N_i \propto a$. The flux from a single bubble is proportional to a times the Nusselt number, i.e., to a^2. But at sufficiently large a/a_r, we have shown that σ_1 is also proportional to a^2. Hence, summing over the relatively large bubbles which contribute significantly, we find that M_v is approximately proportional to the gas flux. Fig. 9 showing the net flux thus demonstrates that the vertically integrated M_v, approximately equal to the net area of bubbles per unit water surface area, has a dominant contribution from bubbles which, at the surface, have radii between 30 and 100 μm, approximately the same range that Fig. 10 showed was important at 1.8 m.

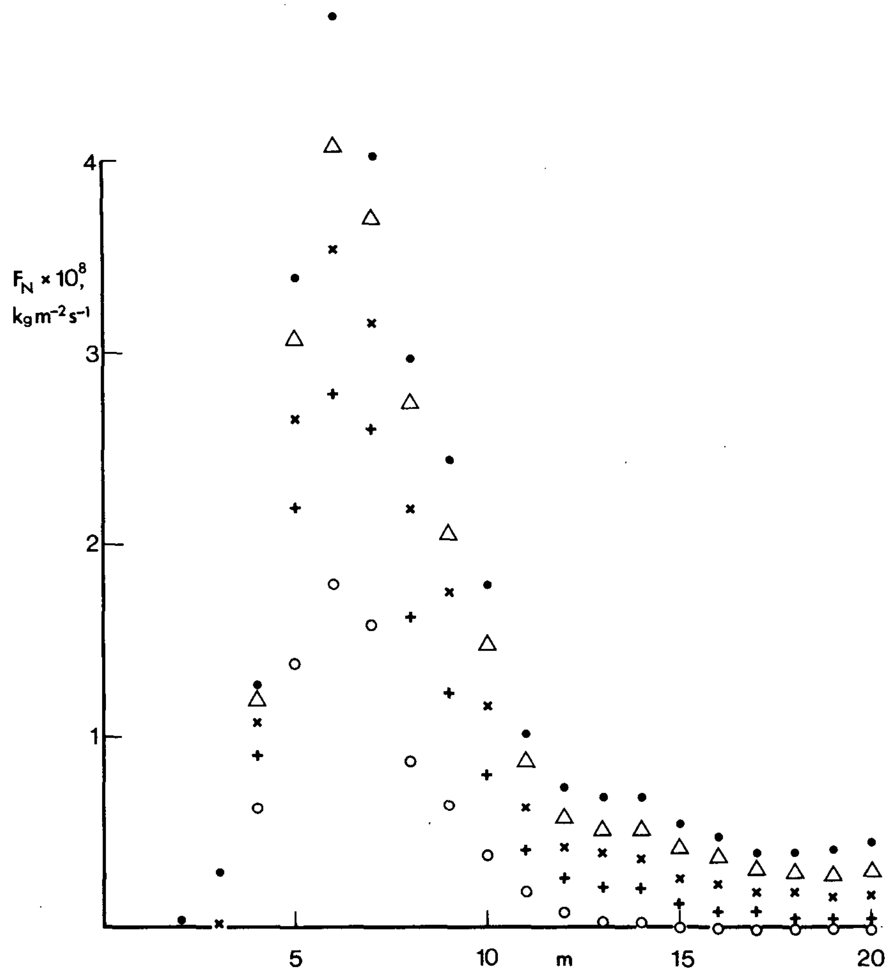

FIG. 9. The flux of nitrogen (F_N) as a function of the size (m) of the input bubbles at K_v = 180 cm² s⁻¹. The symbols represent different saturation levels $s = s_1 = s_2$: −3 (closed circles); 0 (triangles); 3 (crosses); 6 (plus signs); 9 (open circles). The bubble inputs at the surface are the same (S) in each.

The truncation of the model at radii of 200 μm at large values of K_v may produce errors in the estimates of M_v; as K_v increases, larger bubbles can be carried by the enhanced turbulent motions. Fig. 5a suggests that it might be more realistic to extend the input with a uniform size input for $m > 20$. This did not seem worthwhile since the appropriate variation with wind speed is unknown.

The relation between $d(15)$ and K_v might be inverted and used as a means of estimating K_v (see Thorpe, 1984a). Eq. (16) may be regarded as a sensitivity relationship defining the accuracy to which estimates of K_v might be determined if s and D were known with errors Δs and ΔD. Continuous measurement of s_1 or s_2 in the ocean surface water is difficult, but since (16) suggests that errors of 3% in saturation level give rise to errors of less than 10% in K_v it may be possible to estimate K_v to a useful accuracy from sonar measurements of d alone and without monitoring s_1 and s_2. Variations of D in the near-surface ocean will occur as a result of salinity or temperature changes. An undetected variation of 10% would lead to a 3.5% error in K_v. Variation in other coefficients, ν and K_i, will lead to errors of similar magnitude. The importance of variation in γ is more difficult to assess in useful measure owing to the absence of reliable information about the nature of the surface of small bubbles in the sensitive range 30–100 μm. Since however surface tension plays a significant role only for bubbles of radii less than about 20 μm (see I, Sections 3.4 and 5) its variation seems unlikely to lead to great uncertainty in the estimation of K_v from d. The coefficient of ΔK_v in (16) also depends on the input distribution of bubbles, but does not appear to be very sensitive to it. A change of less than 20% occurred at 2 m under conditions of extreme variation of input distribution from the strongly peaked S to a uniform input. Precise determination of K_v may depend on the appropriate

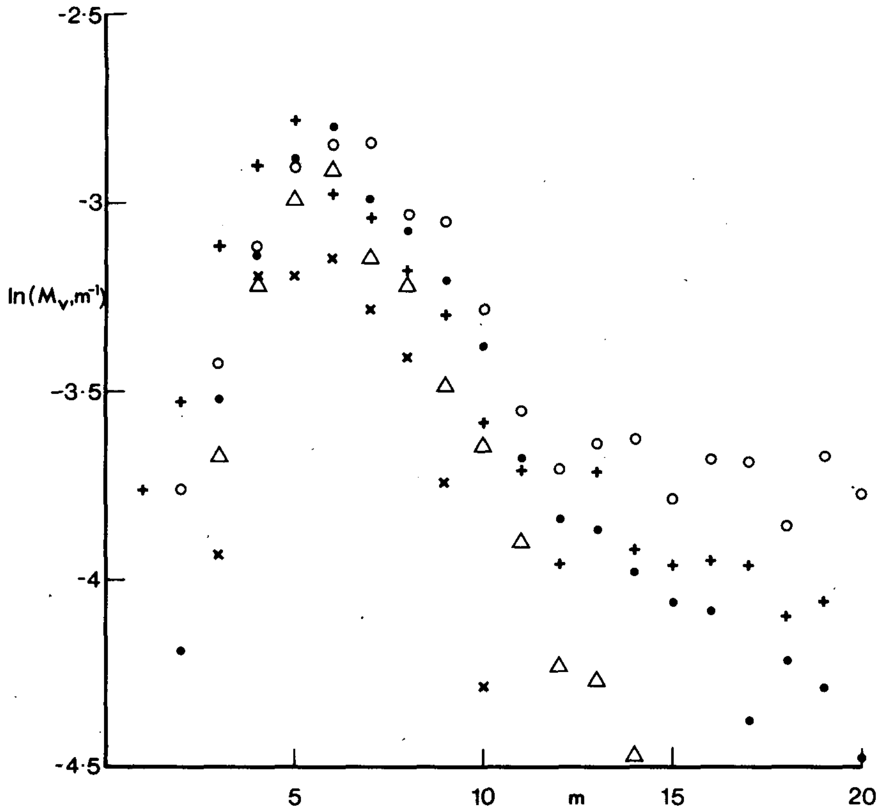

FIG. 10. The contributions of the size of bubble introduced (m) to the acoustic scattering cross-section per unit volume (M_v) at 1.8 m for various values of K_v at $s_1 = s_2 = 0$; $\ln M_v$ is shown. The points represent the following values of K_v (cm^2 s^{-1}): 80 (crosses); 125 (triangles); 180 (closed circles); 245 (plus signs); 320 (open circles).

modeling of the input. If however the input retains a similar form as wind speed varies, it should be possible to achieve high relative accuracy in the estimation of K_v.

The model predicts fairly well the number of bubbles per unit volume at the depths at which JC made observations, but the modeled peak tends to smaller radii as depth increases. This discrepancy is cause for concern. It appears not to be due to incorrect estimation of D (see Fig. 6), and is unlikely to be due to poor estimation of s_i (see Fig. 3) although the saturation levels were not reported by JC. Nor does it seem to be due to inappropriate selection of K_v (see Fig. 7). The tendency of the distribution peak to move to smaller radii as depth increased was found in I when K_v was allowed to vary in proportion to depth and this, together with the present results, provide *prima facie* evidence that the representation of turbulence is not a cause of the discrepancy. We must examine the assumptions of the model and the observations themselves.

Coalescence has been shown to have a negligible effect beyond the neighborhood of the breaking waves provided that the bubble numbers reported by JC are typical (see Thorpe, 1984d). If in infrequent, but dense, bubble clouds the density is two orders of magnitude greater than the mean, coalescence could perhaps be important particularly in fresh water where it occurs more readily. This possibility is suggested by the large variation found in M_v as bubble clouds pass the sonar (see I), and deserves more careful study. Langmuir circulation could also play a role, either by producing effects not represented by K_v in the model, or by biasing the observations. Floating objects, like the floating camera used by JC to record the bubbles, tend to move into regions of convergence, the wind rows, where the concentration of bubbles is higher than average (Thorpe and Hall, 1983) and where there is a mean downward flow. What effect this would have on the distribution of bubbles is discussed elsewhere (Thorpe, 1984c). There is a need for more direct observations of the distribution of bubble sizes in the ocean.

We do not pretend that the present model provides a description of bubbles in the near-surface ocean suitable for prediction of M_v or the gas flux. It fails in the locality of a breaking wave. It is therefore unsuited to provide information about bubbles near their source which could be compared with Koga's (1982) description of bubbles carried to depths of about half the height of the breaking wave by a local circulation in-

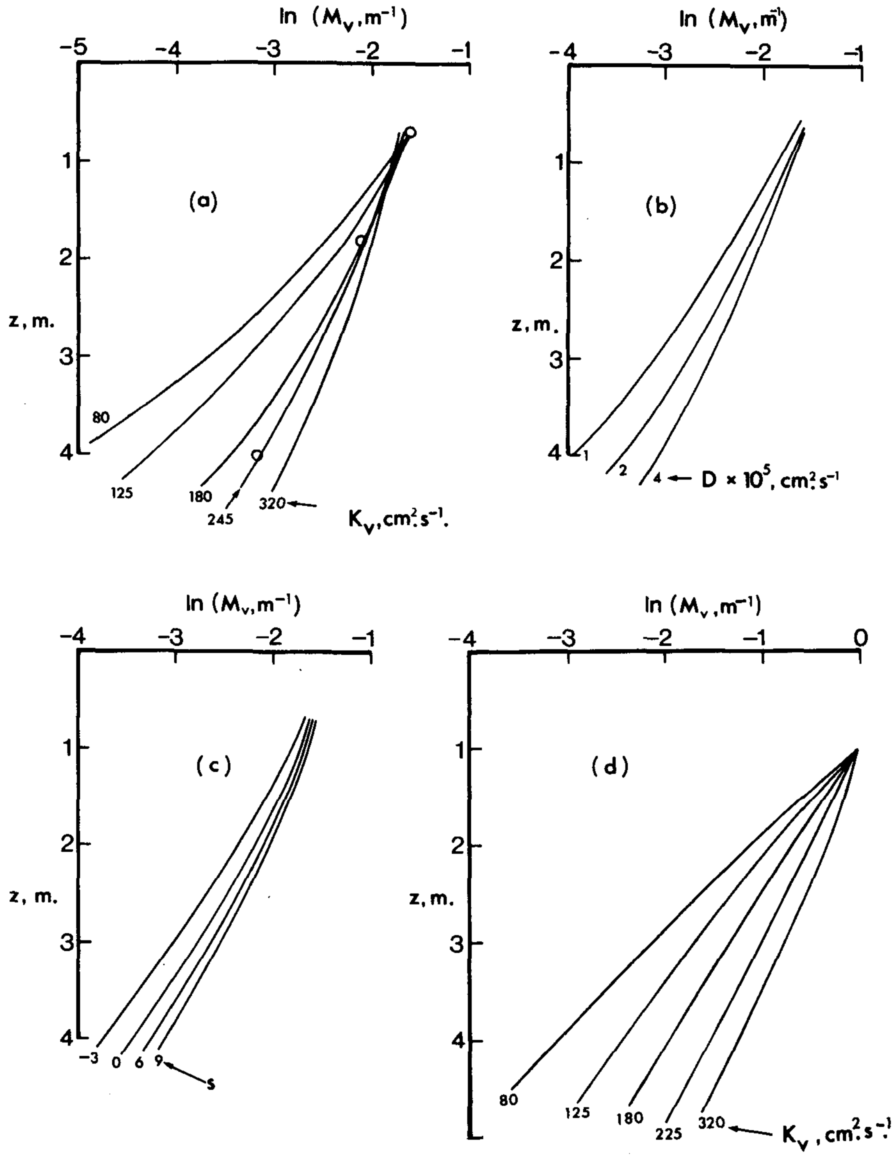

FIG. 11. $\ln M_v$ versus depth, z, for (a) Various K_v at $s = 0$; (b) Various D at $K_v = 180$ cm^2 s^{-1}, $s = 0$; (c) various s at $K_v = 180$ cm^2 s^{-1}; with an input distribution S. The circles in (a) show values of M_v calculated from Johnson and Cooke's observations. (d) The corresponding curves for various K_v at $s = 0$ with the input which has the same number of bubbles of each size. In this case M_v is normalized to unity at $z = 1$ m.

duced in the wave itself. It does however shed some light on the way bubble sizes produced by breaking waves may contribute to the distributions at greater depths. Comparison with available sonar data (in I) shows that the shape of the $\ln M_v$ versus depth curves (Fig. 11a) is unlike that which is observed. The predicted values of M_v differ from estimates based on JC data (the circles in Fig. 11a) which themselves agree with sonar measurements (see I). The difference is most probably because the assumed form of K_v, uniform with depth, is unrealistic. The principal value of this model is that, as mentioned in Section 1, it includes certain effects which could not easily be incorporated in models based on a diffusion equation. We show in the following paper (Thorpe, 1984a) that it provides results consistent with the diffusion models. This strengthens our confidence that we are indeed justified in neglecting these effects. It suggests moreover that results based on the use of diffusion models, perhaps with selections of K_v different from those used here, are sound.

Acknowledgment. This paper was first drafted while the author was a visitor at the School of Oceanography, Oregon State University at Corvallis, and he wishes to thank his hosts, especially Doug Caldwell and Tom Dillon, for inviting him. Partial support was received from the Office of Naval Research Contract N00014-79-C-0004.

REFERENCES

Aleksandrov, A. P., and E. S. Vaindruk, 1974: *The Investigation of the Variability of Hydrophysical Fields in the Ocean,* R. Ozmidov, Ed., Moscow: Nauka Publishing Office, 122–128.

Blanchard, D. C., and A. H. Woodcock, 1957: Bubble formation and modification in the sea and its meteorological significance. *Tellus,* **9,** 145–158.

Csanady, G. T., 1973: *Turbulent Diffusion in the Environment.* Reidel, 248 pp.

Devin, C., 1959: Survey of thermal, radiation and viscous damping of pulsating air bubbles in water. *J. Acoust. Soc. Amer.,* **31,** 1654–1667.

Drogaris, G., and Weiland, P., 1983: Studies of coalescence of bubble pairs. *Chem. Eng. Commun.,* **23,** 11–26.

Garrettson, G. A., 1973: Bubble transport theory with application to the upper ocean. *J. Fluid Mech.,* **59,** 187–206.

Johnson, B. D., and R. C. Cooke, 1979: Bubble populations and spectra in coastal waters: a photographic approach. *J. Geophys. Res.,* **84,** C7, 3761–3766.

——, and ——, 1980: Organic particle and aggregate formation resulting from dissolution of bubbles in seawater. *Limnol. Oceanol.,* **25,** 653–661.

Koga, M., 1982: Bubble entrainment in breaking wind waves. *Tellus,* **34,** 481–489.

Leibovich, S., 1983: The form and dynamics of Langmuir circulations. *Annual Review of Fluid Mechanics,* Vol. 15, Annual Reviews, 391–427.

Lessard, R. S., and Zieminski, S. A., 1971: Bubble coalescence and gas transfer in aqueous electrolytic solutions. *Ind. Eng. Chem. Fundam.,* **10,** 260–269.

Longuet-Higgins, M. S., and J. S. Turner, 1974: An "entraining plume" model of a spilling breaker. *J. Fluid Mech.,* **63,** 1–20.

Mason, B. J., 1971: *The Physics of Clouds.* Clarendon Press, 671 pp.

Monahan, E. C., and I. G. O'Muircheartaigh, 1980: Optimal power-law description of oceanic whitecap coverage dependence on wind speed. *J. Phys. Oceanogr.,* **10,** 2094–2099.

Scott, J. C., 1975: The role of salt in whitecap persistence. *Deep-Sea Res.,* **22,** 653–657.

Thorpe, S. A., 1982: On the clouds of bubbles formed by breaking wind-waves in deep water, and their role in air-sea gas transfer. *Phil. Trans. Roy. Soc. London,* **A304,** 155–210.

——, 1984a: On the determination of K_v in the near-surface ocean from acoustic measurements of bubbles. *J. Phys. Oceanogr.,* **14,** 855–863.

——, 1984b: The effect of bubbles produced by breaking wind-waves on gas flux across the sea surface. *Ann. Geophys.,* **2,** 53–56.

——, 1984c: The effect of Langmuir circulation on the distribution of submerged bubbles caused by breaking wind waves. *J. Fluid Mech.,* **142,** 151–170.

——, 1984d: Bubble clouds: a review of their detections by sonar, of related models, and of how K_v may be determined. *Oceanic Whitecaps and their Role in Air-Sea Exchange Processes,* E. C. Monahan and G. MacNiocaill Eds., Galway University Press (in press).

——, and P. N. Humphries, 1980: Bubbles and breaking waves. *Nature,* **283,** 463–465.

——, and A. J. Hall, 1983: The characteristics of breaking waves, bubble clouds, and near-surface currents observed using side-scan sonar. *Cont. Shelf Res.,* **1,** 353–384.

Urick, R. J., 1975: *Principles of Underwater Sound.* McGraw-Hill, 384 pp.

Wu, J., 1979: Oceanic whitecaps and sea state. *J. Phys. Oceanogr.,* **9,** 1064–1068.

Wyman, J., P. F. Scholander, G. A. Edwards and L. Irving, 1952: The stability of gas bubbles in sea water. *J. Mar. Res.,* **11,** 47–62.